



Parameterization of a diagnostic carbon cycle model for continental scale application

David A. King, David P. Turner^{*}, William D. Ritts

Forest Ecosystems and Society, Oregon State University, Corvallis OR, USA

ARTICLE INFO

Article history:

Received 13 September 2010
Received in revised form 24 February 2011
Accepted 27 February 2011
Available online 6 April 2011

Keywords:

Carbon flux
Diagnostic model
FPAR
EVI
Light use efficiency
Parameter optimization
CFLUX
Gross primary production
Ecosystem respiration
Net ecosystem production
Eddy covariance flux tower

ABSTRACT

Diagnostic carbon cycle models depend on parameterization to establish model sensitivity to climate variables and site factors. Here we acquired meteorological and carbon flux data from a diverse set ($N = 18$) of eddy covariance (EC) flux towers, along with MODIS data on FPAR (the fraction of incident photosynthetically active radiation that is absorbed by the plant canopy) at the sites, and used the data to develop a parameter set for the application of a diagnostic carbon cycle model over North America. The parameter optimization approach relied on goodness of fit between model simulations and tower estimates of gross primary production and net ecosystem production (NEP). Parameters such as light use efficiency (LUE) and base rate of heterotrophic respiration varied widely between sites representing different plant functional types (PFTs), thus supporting the value of stratification by PFT when parameterizing the model. Where multiple EC sites were available within a PFT, overall prediction error and bias in mean NEP was reduced by cross-site optimization as opposed to reliance on a single site. Optimization with the MODIS Enhanced Vegetation Index (EVI) instead of MODIS FPAR resulted in a similar goodness of fit, however, LUE values were pushed to levels that were not physiologically realistic when using EVI. The increasing availability of gap-filled EC tower data is rapidly improving the opportunities for direct coupling of satellite and ground observational data for parameterizing of diagnostic carbon flux models.

© 2011 Elsevier Inc. All rights reserved.

1. Introduction

The combination of satellite imagery, distributed climate data, and diagnostic process-based carbon cycle models offers the opportunity for indirect estimation of terrestrial carbon flux over large areas in a spatially-explicit manner (Running et al., 1999; Turner et al., 2004). Critical model inputs may include vegetation cover type (Friedl et al., 2010), disturbance history (Kennedy et al., 2007), FPAR (the fraction of incident photosynthetically active radiation that is absorbed by the plant canopy, Myneni et al., 2002), and leaf phenology (Zhang et al., 2006). Model application generally requires that various parameters be specified. Thus, observations in addition to the remote sensing data can be introduced in the parameterization process to constrain carbon flux estimates.

Eddy covariance (EC) flux towers (Baldocchi et al., 2001) make measurements of net ecosystem exchange (NEE) of CO_2 , with partitioning into its gross primary production (GPP) and ecosystem respiration (R_e) components, which are particularly relevant to diagnostic model parameterization. Most directly, tower estimates of GPP and PAR (photosynthetically active radiation) absorbed by the

canopy are used to estimate light use efficiency (LUE), a key variable in many diagnostic models (McCallum et al., 2009). Surveys of vegetation LUE over a range of biome types and plant functional types have revealed significant variation depending on vegetation type (Garbulsky et al., 2010; Gower et al., 1999; Turner et al., 2003). EC tower observations of GPP can also be the basis for optimizing model parameters that control the influence of environmental drivers like temperature and vapor pressure deficit (VPD) on LUE.

Optimization of parameters in algorithms for simulating heterotrophic respiration (R_h) can likewise be accomplished with tower data. In so called “data driven” approaches (e.g. Mahadevan et al., 2008), the R_h algorithm relies on a base rate that is modified by environmental variables such as temperature and soil moisture. These models are much faster to run than diagnostic models that account for carbon stocks, i.e. the C stock models may require “spin-up” of hundreds to thousands of years to bring soil C pools into near equilibrium with local climate (Potter et al., 1993). Because of their relative simplicity and fast run time, the data driven models are amenable to comprehensive parameter optimization (Turner et al., 2006; Wang et al., 2009).

Relatively simple diagnostic flux models also make it possible to optimize model parameters within an inversion modeling framework (Göckede et al., 2010a, 2010b). In that case, spatially and temporally distributed observations of CO_2 concentration are brought to bear on the process of surface flux estimation. In combination, observations of FPAR, NEE, and CO_2 concentration are potentially a powerful constraint on simulated surface carbon flux.

^{*} Corresponding author at: Department of Forest Ecosystems and Society, Oregon State University, Corvallis OR 97331-7501, USA. Tel.: +1 541 737 5043; fax: +1 541 737 1393.

E-mail address: david.turner@oregonstate.edu (D.P. Turner).

Research issues associated with diagnostic model development include designing effective model algorithms, parameterizing the models, assessing their sensitivity to spatial variation in the inputs, evaluating the effectiveness of various remote sensing inputs, and validating model-based flux estimates. Of special concern when optimizing with tower data is the sensitivity of these models to environmental variation away from the reference tower sites. In this study, we acquired meteorological and carbon flux observations from a diverse set of EC flux towers, along with MODIS data for these sites, and performed a parameter optimizing exercise for an existing diagnostic model (CFLUX, Turner et al., 2006). For plant functional types (PFTs) with multiple EC sites within a climate zone, we evaluated multi-site vs. single site optimizations. Follow-up analyses included evaluating the effectiveness of the MODIS Enhanced Vegetation Index (EVI) compared to the effectiveness of the standard MODIS FPAR product across this wide range of sites. EVI was developed to reduce the degree of saturation found in other vegetation indices (Huete et al., 2002) and has been used in several net ecosystem production (NEP) scaling approaches (Mahadevan et al., 2008; Matross et al., 2006; Xiao et al., 2010). We have previously used this modeling framework to assess alternative sources of FPAR data (Turner et al., 2009). Our motivation for these new analyses was to develop a PFT/climate zone-specific parameter set for projecting NEP across North America.

2. Methods

2.1. Overview

The CFLUX model calculates daily GPP as the product of absorbed photosynthetically active radiation and LUE, where the latter is influenced by site factors, meteorological variables, and soil water content. Autotrophic respiration (R_a) is a fixed proportion of GPP. R_h is dependent on site, stand age (for forests), soil temperature and water content, and FPAR. Eight adjustable parameters (5 for GPP and 3 for NEP) were optimized by minimizing root mean square error (subject to parameter constraints) to fit daily GPP and NEP using 18 EC flux tower sites, chosen to include the major PFTs and climate zones across

North America. Tower-based GPP was derived from daytime NEE and estimates of daytime R_e based on daytime temperatures and the relationship of nighttime NEE to temperature (Turner et al., 2005). The optimized parameters specify maximum light use efficiency and the effects of temperature and VPD on GPP as well as the base rate and temperature dependence of R_h . As we assume that NPP/GPP is a constant fraction for each site, R_h is related to the flux tower estimates of daily GPP and NEP by $R_h = NEP - NPP$. The locations of the sites in relation to the PFTs (based on Friedl et al., 2010), and the climate zones (based on Omernik, 1987) are shown in Fig. 1. Subsequent to parameter optimization, we examined the model error and parameter uncertainty, and the sensitivity of the predicted annual fluxes to altered climate and soil water holding capacity. We also compared cross-site model parameterizations to single site fits and use of EVI instead of FPAR. The central algorithms of CFLUX are presented here, emphasizing the role of the optimized parameters. A complete description of the model is given in Turner et al. (2006).

2.2. Model description

CFLUX simulates daily GPP, R_a , R_h , and NEP from meteorological inputs, satellite estimates of vegetation greenness, and a daily soil water balance. Daily meteorological inputs are total precipitation, average temperature (Tavg), minimum temperature (Tmin), soil temperature (Tsoil), photosynthetically active radiation (PAR), and daytime mean vapor pressure deficit (VPD). Site variables include plant functional type and plant available water at field capacity, i.e., soil water holding capacity (WHC), as well as stand age and original disturbance type (fire or harvest) in the case of forests. All of the daily carbon fluxes are given in units of $gC\ m^{-2}\ d^{-1}$. Annual fluxes are the sums of daily fluxes.

Light use efficiency, as affected by environment, is central to estimating GPP and is specified as

$$GPP = LUE_f * PAR * FPAR \quad (1)$$

where GPP is gross primary production ($gC\ m^{-2}\ d^{-1}$), LUE_f is the final light use efficiency ($gC\ MJ^{-1}$), PAR is incident photosynthetically

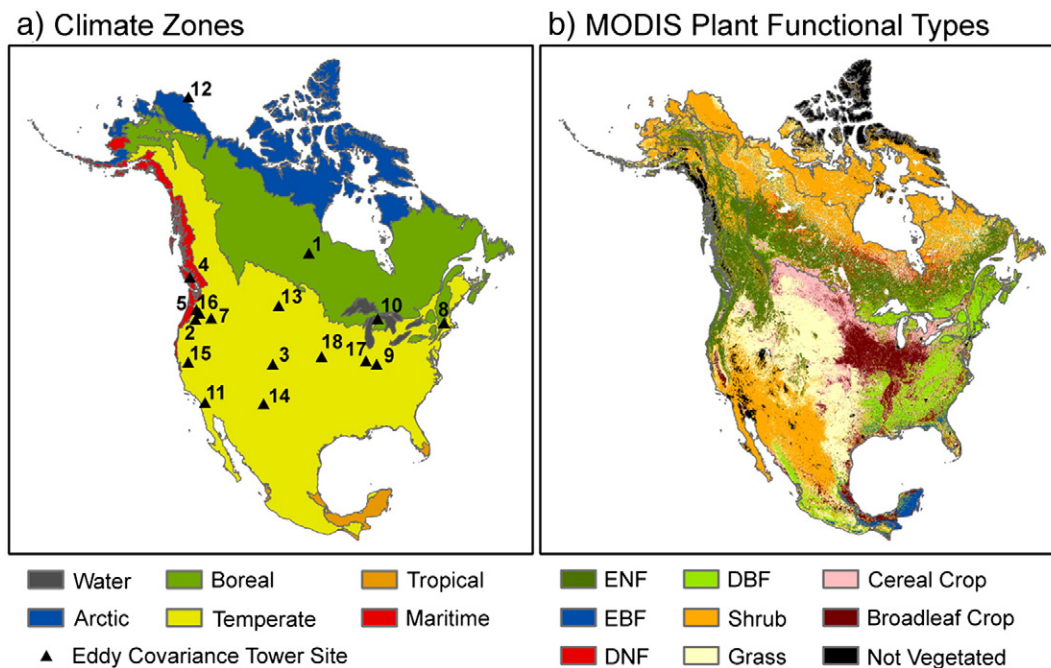


Fig. 1. Climate zones and Plant Functional Types (PFTs) over North America. a) Climate zones based on ecozones of Omernik (1987), b) PFTs from MODIS (Friedl et al., 2010). Eddy covariance sites used in the study are indicated by triangles. Site numbers are the same as in Table 1.

active radiation ($\text{MJ m}^{-2} \text{d}^{-1}$), and FPAR is the fraction of PAR absorbed by the canopy. CFLUX calculates an initial daily light use efficiency that varies with fractional cloud cover, which is estimated from the ratio of PAR to POTPAR (potential clear sky PAR) for each day of the year. This initial LUE varies linearly from a minimum clear sky value to a maximum for completely overcast days. To calculate the final light use efficiency of Eq. (1), the initial LUE is reduced by multipliers that incorporate limitations on photosynthesis due to low night temperatures, soil moisture deficits, high VPD, and in the case of forests, stand age.

That is,

$$LUE_f = LUE_{base} * S_{Tmin} * S_{SWg/VPD} * S_{Sag} \quad (2)$$

where

- S_{Tmin} minimum temperature scalar
- $S_{SWg/VPD}$ the smaller of the soil water scalar for GPP (S_{SWg}) or the VPD scalar (S_{VPD})
- S_{Sag} stand age scalar for GPP, which reduces LUE as stand age increases above a certain minimum age, depending on forest type.
- LUE_{base} initial LUE as influenced by cloudiness, i.e.

$$LUE_{base} = (LUE_{max} - LUE_{cs}) * S_{CI} + LUE_{cs} \quad (3)$$

where

- S_{CI} cloudiness index scalar that varies from 0 on clear days to 1 on fully overcast days and is inferred from the PAR/POTPAR ratio (Turner et al., 2006).
- LUE_{cs} initial LUE for clear sky days.
- LUE_{max} initial LUE for overcast days.

All scalars take on values ≤ 1 , depending on environmental conditions.

Regarding Eq. (2), S_{Tmin} has a value of 0 when $T_{min} \leq T_{min,min}$ and increases linearly to 1 at temperature $T_{min,max}$. Similarly, the VPD scalar (S_{VPD}) has a value of 1 when $VPD \leq VPD_{min}$ and declines linearly to zero as VPD increases to VPD_{max} (Running et al., 2000). The soil water scalar (S_{SWg}) depends on SW, the ratio of current plant available water to plant available water at field capacity. $S_{SWg} = 1$ when this ratio is > 0.5 and declines linearly to 0.2, as SW declines from 0.5 to 0.1,

at which value it remains for $SW < 0.1$. To track SW, the model performs a simple water balance by estimating daily evapotranspiration based on the site-specific inverse of water use efficiency. The age scalar, (S_{Sag}) is equal to 1 for non-forest vegetation types and very young forests. Above a specified minimum age, S_{Sag} declines asymptotically to a value of 0.66–0.82, depending on forest type (Turner et al., 2006).

The clear sky LUE (LUE_{cs}) of Eq. (3) is specified for each site or climate zone by PFT combination based on observations of LUE at eddy covariance flux towers. LUE under low stress conditions is plotted (e.g. Fig. 2) as a function of PAR/POTPAR (decreasing cloud cover) and clear sky LUE is based on the value when PAR/POTPAR approximates 1.0.

Total respiration (R_e) is the sum of R_a and R_h . In CFLUX, R_a can be calculated as either the sum of growth plus maintenance respiration or from the assumption of a constant NPP/GPP ratio. We have chosen the latter approach, based on observations that the ratio of annual NPP/GPP tends to be stable within plant functional types and climate zones (De Lucia et al., 2007). Also, the Q_{10} of 2 often used to model the temperature dependence of maintenance respiration at a given site does not apply across sites of varying climate (Atkin & Tjoelker, 2003). Hence, for a continent-wide assessment based on a sparse network of flux towers, the constant NPP/GPP assumption is likely to produce less error.

As with LUE, R_h is calculated in terms of a base rate and multiplicative scalars related to soil temperature, soil moisture and stand age. FPAR is also included as a multiplier in calculating R_h , given the observation that soil respiration is correlated with recent photosynthetic production, which is coupled with FPAR (Hogberg et al., 2001). That is,

$$R_h = R_{h_base} * S_{STh} * S_{SWh} * S_{SAh} * FPAR_h \quad (4)$$

where

- S_{STh} scalar for soil temperature.
- S_{SWh} scalar for the effects of plant available soil water on heterotrophic respiration.
- S_{SAh} stand age scalar for heterotrophic respiration.
- $FPAR_h$ the smaller of FPAR or $FPAR_{min}$, the latter specified to permit soil respiration outside the growing season for vegetation types with a leafless dormant period.
- R_{h_base} rate of heterotrophic respiration at a temperature of 0 °C, when the soil water is at field capacity and both $FPAR_h$ and $S_{SAh} = 1$, the latter being the case for non-forest vegetation.

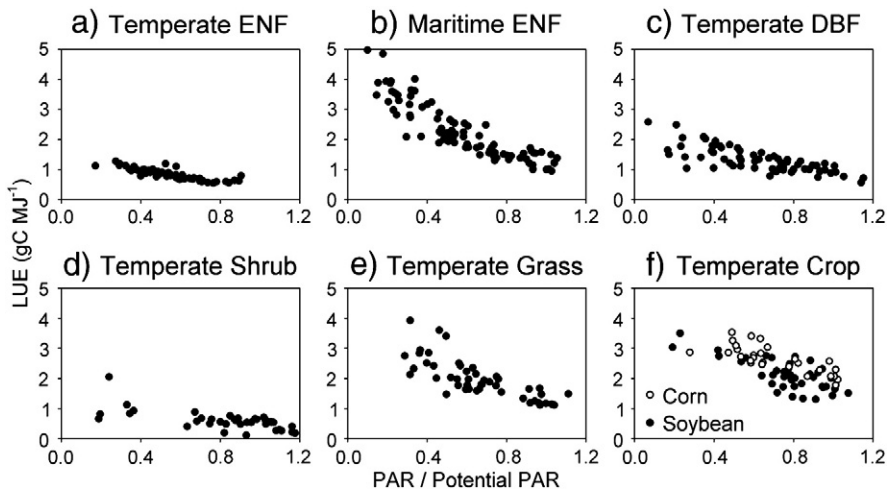


Fig. 2. Light use efficiency (LUE) under low stress conditions illustrated for representative years for six of the PFTs. PAR = daily photosynthetically active radiation, Potential PAR = daily clear sky PAR, uncorrected for humidity effects (Fu & Rich, 1999; Turner et al., 2006). Sites and years are a) 3/2002, b) 4/2002, c) 9/2005, d) 11/2005, e) 15/2003, f) 18/2002 soybean, 2005 corn, as listed by site number in Table 1.

All respiration associated scalars have a value ≤ 1 , depending on environmental conditions, with the exception of S_h , which varies exponentially with soil temperature and has a value of 1 at 0 °C. That is,

$$S_{STh} = \exp(R_{h_coef_a} * T_{soil}) \quad (5)$$

where $R_{h_coef_a}$ is an optimized parameter. The heterotrophic soil water scalar is given by

$$S_{SWH} = \left(1 - b * e^{(-c * SW)}\right) / d \quad (6)$$

where $SW = (\text{plant available water}) / (\text{plant available water at field capacity})$, $b = 0.86$, $c = -1.26$ and $d = 0.7486$ for all vegetation types (Turner et al., 2006). Thus, heterotrophic respiration declines with decreasing soil water, but in a different fashion than does LUE, which is unaffected for $SW > 0.5$. The heterotrophic age scalar for forests is given by

$$S_{SAh} = a \left[0.5 + b * e^{(c * \text{age})} + 0.5(1 - d^{\text{age}}) \right] \quad (7)$$

where $a = 0.379$, $b = 2.14$, $d = 0.9824$, and $c = -0.158$ for stands originating after logging or $c = -0.07$ for fire regenerated stands. This function yields the higher respiration expected in young stands due to decomposing debris following disturbance, particularly in fire regenerated stands, where fire-killed trees remain on site. The latter difference is mediated by the altered value of c . The parameter values defining S_{SAh} are based on those of Turner et al. (2006) for interior western conifers, with a minor adjustment to insure that fire and logging originated stands converge to the same heterotrophic respiration in old age.

2.3. Parameter optimization

CFLUX has two sets of parameters that may be optimized; five parameters that affect GPP and three affecting R_h . The optimized GPP parameters are LUE_{max} and those determining the responses to T_{min} (T_{min_min} and T_{min_max}) and VPD (VPD_{min} and VPD_{max}). The optimization also checks the case of omitting each of the scalars from the algorithm. The optimized R_h parameters are R_{h_base} , $R_{h_coef_a}$ and $FPAR_{min}$. We used the parameter ranges and increments of Turner et al. (2006), with the exception of LUE_{max} , which had been limited to 4 gC MJ^{-1} , the approximate maximum efficiency of photosynthesis (Haxeltine & Prentice, 1996). We removed this upper bound because the EVI input (see below) was often much lower than the actual FPAR, thus requiring a higher LUE to match observed GPPs. For purposes of consistent comparison we also removed the upper bound for the MODIS FPAR optimizations, though the resulting LUE_{max} values seldom exceeded 4 gC MJ^{-1} .

The parameter sets minimizing the annual root mean square error (RMSE) in daily GPP and NEP were determined by first running CFLUX with a 5-dimensional grid of GPP parameters and then a 3 dimensional grid of R_h parameters—using the optimal set of GPP parameters for the latter runs. This computationally intensive approach is feasible with simple diagnostic models and allows for visual inspection of the associated errors. In optimizing the parameters we incremented LUE by 0.1 gC MJ^{-1} , T_{min_min} and T_{min_max} by 2 °C , VPD_{min} and VPD_{max} by 500 Pa , R_{h_base} by $0.1 \text{ gC m}^{-2} \text{ d}^{-1}$, $R_{h_coef_a}$ by 0.01 and $FPAR_{min}$ by 0.1 (the latter two are both dimensionless). We used these rather coarse increments, given the 5 dimensional grid for GPP and our observation that the RMSE was generally insensitive to the parameters close to the optimum.

2.4. FPAR and EVI data

We obtained MODIS (Collection 5) FPAR (1 km) and EVI (250 m) for each tower site from Oak Ridge National Laboratory (2010). Temporal gaps of low quality data were filled using the algorithm in Zhao et al. (2005). Following Wu et al. (2010), values for each 8 day period were averaged over the $3 \text{ km} \times 3 \text{ km}$ cell area centered on each tower.

2.5. Site level initialization and reference flux data

The tower sites and characteristics of the associated vegetation are shown in Table 1. In the cases of the deciduous needleleaf forest PFT in the temperate zone and the cereal PFT in the temperate zone, we were unable to locate usable EC tower carbon flux data. Thus in these cases, the Biome-BGC model (Thornton et al., 2002) was run at a location within the temperate climate zone supporting the relevant PFT, and outputs of GPP and NEP were used for reference data (as in Turner et al., 2006). Site measurements of daily T_{avg} , T_{min} , T_{soil} , precipitation, PAR and daytime mean vapor pressure deficit (VPD) were used as model inputs. Tower data was directly from tower operators in 9 cases and from AmeriFlux (2011) in 7 cases (Level 4).

The clear sky LUE varied substantially among sites, being low for high elevation conifers of the Rocky Mountains (site 3) and the dry California chaparral (site 11). At one of the crop sites, LUE was higher during the year that corn was grown than when soybean was grown (Fig. 2). This pattern is expected, as the beans of soybean are ~20% oil and oil has a lower carbon content and twice the energy content of carbohydrate.

The NPP to GPP ratio was based on the comprehensive review of measured values by De Lucia et al. (2007) except for the old-growth temperate maritime coniferous forest (site 5), which used Harmon et al. (2004). The inverse water use efficiency ($1/WUE$) denotes ET (measured as depth of water used) per unit of GPP. Average annual values of $1/WUE$ were estimated from the compilation of Law et al. (2002) for a range of PFTs and from measurements of ET at some of the sites (Garbulsky et al., 2010; Thomas et al., 2009). $1/WUE$ was typically about $0.3 \text{ mm H}_2\text{O gC}^{-1} \text{ m}^{-2}$ ($= 0.3 \text{ kg H}_2\text{O gC}^{-1}$) for temperate deciduous broadleaf forests and crops and substantially higher for dry chaparral (site 11) and arid grasslands (site 14), where high VPDs and a higher fraction of water lost to surface evaporation result in higher ET per unit of carbon fixed (Law et al., 2002).

Soil water holding capacity (WHC) was determined primarily from reported soil properties at the sites (cited in Table 1). The high value of 800 mm for the Amazonian tropical forest (site 6) is supported by evidence of deep rooting here (da Rocha et al., 2004; Nepstad et al., 1994) and the fact that observed GPP did not decline as modeled soil moisture deficits approached 400 mm. The second highest value of 400 mm for the Pacific Northwest temperate evergreen needleleaf forest (site 2) is associated with the high drought tolerance and deep rooting habit of *Pinus ponderosa* (Licata et al., 2008; Oliver & Ryker, 1990), the canopy species of this site.

3. Results

3.1. Site-level optimizations with MODIS FPAR

The optimized parameters for each site are based on optimizations across 1–4 years of observations (Table 2). The LUE_{max} values defining the base LUE for overcast days were commonly 2–3 times the corresponding clear sky LUE values (Tables 1 and 2), consistent with the patterns of Fig. 2 and the general observation of higher LUE's under low intensity, diffuse light than during bright clear days that saturate sunlit leaves (Choudbury, 2001; Hollinger et al., 1994). Note that this shift in LUE may be due mainly to differences in light intensity rather than light quality at a given intensity (Alton et al.,

Table 1

Eddy-covariance flux tower sites used in this study. Site locations shown in Fig. 1. PFT = Plant Functional Type. 1/WUE = inverse of water use efficiency, WHC = Water holding Capacity. ENF = Evergreen Needleleaf Forest, DNF = Deciduous Needleleaf Forest, DBF = Deciduous Broadleaf Forest. NA = Not Applicable.

Site no.	Site code	Climate ^a zone	PFT ^a	Site variables					Reference
				LUE _{cs} (gC MJ ⁻¹)	NPP/GPP	1/WUE (mm H ₂ O gC ⁻¹ m ⁻²)	WHC (mm)	Stand age (y)	
1	NOBS	Boreal	ENF	1.0	0.3	0.33	200	160	Dunn et al. (2007)
2	METI	Temperate	ENF	0.9	0.4	0.3	400	80	Thomas et al. (2009)
3	NIWO	Temperate	ENF	0.55	0.5	0.4	200	100	Monson et al. (2002)
4	CRIV	Maritime	ENF	1.35	0.5	0.25	300	60	Krishnan et al. (2009)
5	WRIV	Maritime	ENF	1.1	0.3	0.25	200	450	Falk et al. (2008)
6	TAPA	Tropical	EBF	1.5	0.5	0.4	800	200	Saleska et al. (2003)
7	ORL1	Temperate	DNF	0.8	0.5	0.4	200	100	This study
8	HARV	Temperate	DBF	1.3	0.5	0.29	150	90	Urbanski et al. (2007)
9	MORG	Temperate	DBF	1.1	0.5	0.29	150	70	Schmid et al. (2000)
10	UMBS	Temperate ^a	DBF	1.3	0.5	0.29	200	80	Schmid et al. (2003)
11	SKON	Temperate	SHRUB	0.4	0.5	0.6	120	NA	Luo et al. (2007)
12	BARO	Arctic	GRASS	0.45	0.5	0.4	100	NA	Kwon et al. (2006)
13	PECK	Temperate	GRASS	0.9	0.5	0.6	50	NA	Gilmanov et al. (2005)
14	SEVI	Temperate	GRASS	0.6	0.5	0.8	40	NA	Kurc & Small (2007)
15	VAIR	Temperate	GRASS	1.4	0.5	0.4	100	NA	Ma et al. (2007)
16	ORW1	Temperate	CEREAL	0.55	0.6	0.4	120	NA	This study
17	BOND	Temperate	CROP	1.4	0.6	0.3	200	NA	Meyers & Hollinger (2004)
18	MEDR	Temperate	CROP	1.9	0.6	0.3	200	NA	Verma et al. (2005)

^a Climate zone and plant functional type based on Omernik (1987) and Friedl et al. (2010), respectively, with the exception of the University of Michigan Biological Station (UMBS) site, which is in the transition zone between mixed hardwood and boreal forests (Schmid et al., 2003). As this site is now dominated by hardwoods, we classified it as Temperate DBF.

2007). The base respiration rate ($R_{h,base}$) had a wide range among sites, depending in part on site productivity and the value of the temperature exponent ($R_{h,coef,a}$). The base rate tended to be lower for sites with a high temperature dependence of R_h , as a low base rate is needed to produce a given R_h during the warm growing season if the temperature response is large. For PFT/climate zones with multiple sites, the parameters defining the response to minimum temperature tended to be similar across sites (Table 2).

The variation in daily RMSE in GPP and NEP as a function of pairs of the optimized parameters is illustrated in Fig. 3. Typically there appeared to be only one minimum over the examined parameter space and little variation in error about the optimum. That is, small departures from the optimum had little effect on the error, justifying our use of a rather coarse grid of input values. In some cases, the optimum lay at the edge of the examined parameter space (Fig. 3b). For the R_h parameters, the contour plots of RMSE vs. the base respiration rate and the temperature dependence parameter ($R_{h,coef,a}$) showed an elongate diagonal depression, indicating strong covariance in the

effects of these parameters (Fig. 3d). At a given above-zero temperature, the same predicted respiration rate can be achieved by increasing the base rate while decreasing the temperature dependence, so this covariance is expected.

The optimized model tended to track the seasonal patterns and fluctuations in observed NEP at each site, although the day-to-day fluctuations projected by CFLUX were sometimes noticeably smaller than observed (Fig. 4). The daily RMSE of the optimized model was correlated with site productivity ($r = 0.47$ and $r = 0.48$, $p < 0.05$ in both cases for the RMSE in GPP and NEP, respectively), as proportionally greater errors are expected with greater daily fluxes (Table 3). The greatest RMSE values were observed at the CROP sites which showed high GPP (and hence high daily RMSE) during a rather short growing season and involved optimizations for alternative corn and soybean years. As the annual GPP for the corn year was 1.7–2.0 times that for the soybean year, a common optimization will under-predict corn GPP and over-predict soybean GPP. However, the average projected GPP across the corn and soybean years was close to the

Table 2

Parameter values for base case of MODIS FPAR, site level, and cross year. Sites as defined in Table 1. NO (Not Optimized) refers to the case where the optimization yielded as low or lower RMSE without using the related scalar. Sites are defined in Table 1.

Site no.	PFT/climate	No. y	GPP parameters					R _h parameters		
			Tmin _{min} (°C)	Tmin _{max} (°C)	VPD _{min} (Pa)	VPD _{max} (Pa)	LUE _{max} (gC MJ ⁻¹)	R _{h,base} (gC m ⁻² d ⁻¹)	R _{h,coef,a}	MinFPAR
1	ENF/Boreal	2	-10	8	1000	4000	2.7	1.5	0.04	0.7
2	ENF/Temp	4	-12	4	1000	4000	2.4	0.1	0.24	0.5
3	ENF/Temp	4	-8	4	500	3000	1.4	3.0	0.02	0.8
4	ENF/Mar	4	-12	14	1000	4000	4.0	0.8	0.24	0.7
5	ENF/Mar	4	NO	NO	0	3500	3.3	0.5	0.17	0.7
6	EBF/Trop	2	NO	NO	500	3500	4.9	12.2	0.01	0.5
7	DNF/Temp	1	-10	4	2500	4000	1.3	4.1	0.01	1.0
8	DBF/Temp	2	-2	14	1000	1500	4.7	1.8	0.01	1.0
9	DBF/Temp	2	-2	14	1000	4000	2.8	2.9	0.01	1.0
10	DBF/Temp	2	-2	14	500	4000	2.6	3.9	0.01	1.0
11	SHRUB/Temp	2	-6	4	1000	4000	1.0	0.1	0.03	0.5
12	GRASS/Arctic	1	-12	4	0	1500	0.7	0.4	0.01	1.0
13	GRASS/Temp	1	-12	4	2000	3500	2.1	0.2	0.11	1.0
14	GRASS/Temp	2	-12	4	NO	NO	0.9	0.1	0.01	0.7
15	GRASS/Temp	4	-12	6	1000	2500	3.5	2.2	0.03	1.0
16	CEREAL/Temp	1	NO	NO	2500	4000	1.6	0.1	0.20	0.8
17	CROP/Temp	2	-2	14	1000	2000	1.9	0.3	0.07	1.0
18	CROP/Temp	2	-2	14	500	4000	1.9	2.0	0.02	1.0

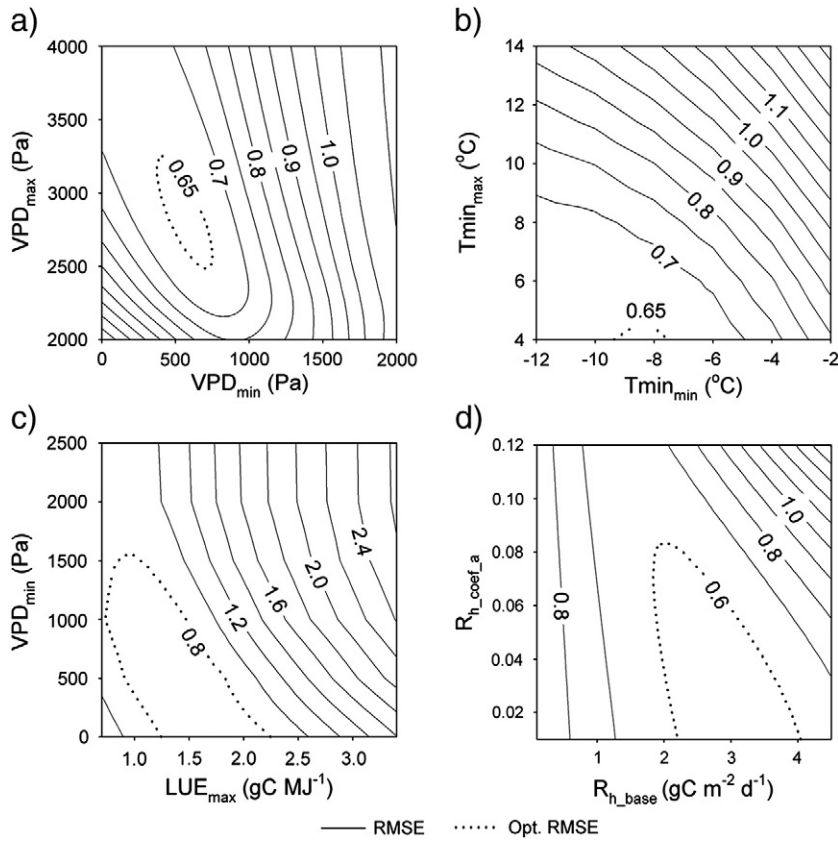


Fig. 3. Cross-year RMSE contours for Temperate ENF (site 3) plotted as functions of the illustrated pairs of optimized parameters. Panels a)–c) show the RMSEs associated with GPP; panel d), the RMSE associated with NEP, following the GPP optimization. Dotted lines show the inner contour containing the optimum parameter set.

observed average at both CROP sites (Table 3), so this parameterization may be unbiased for regions with a patchwork of equal proportions of corn and soybean.

3.2. Model sensitivity to soil properties and climate

The influence of soil properties and climate on the model predictions are illustrated by figures showing the full response of annual GPP, R_e and NEP to soil water and climate variables for selected sites and a table showing the change of these carbon fluxes due to small increments of the soil and climate inputs.

The soil water scalars affecting predicted GPP and heterotrophic respiration are functions of proportional soil water (SW), defined as the ratio of plant available soil water to plant available water at field capacity (WHC). The latter varies with soil texture, depth and vegetation type and its variation across the landscape may thus be difficult to estimate. The effect of changing WHC is illustrated in Fig. 5, based on our standard assumption that soils are at field capacity on January 1, due to recharge of soil moisture during the winter, when rates of evapotranspiration are low. Annual GPP declines curvilinearly as WHC is reduced below a threshold that depends on precipitation and site productivity—as evapotranspiration is directly linked to GPP

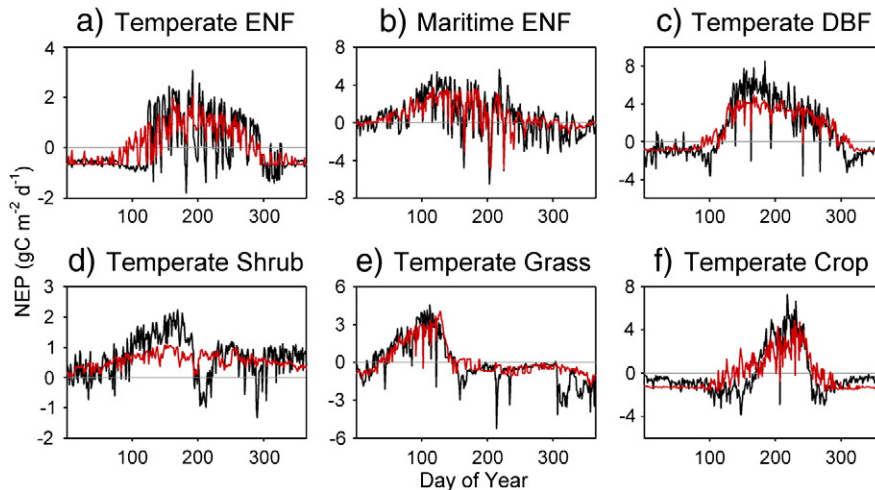


Fig. 4. Time series plots of observed and modeled NEP, indicated by black and red lines, respectively. Sites and years are the same as in Fig. 2 (soybean year for panel f).

Table 3

Observed (Tower) and simulated (CFLUX) annual fluxes and RMSEs for gross primary production (GPP) and net ecosystem production (NEP) in the base case simulations. Flux values are means across years in the cases of multi-year simulations. NA = Not Applicable (at these sites only growing season fluxes were measured). Sites are defined in Table 1.

Site no.	Tower GPP _{annual} (gC m ⁻² y ⁻¹)	CFLUX GPP _{annual} (gC m ⁻² y ⁻¹)	RMSE _{GPP} (gC m ⁻² d ⁻¹)	Tower NEP _{annual} (gC m ⁻² y ⁻¹)	CFLUX NEP _{annual} (gC m ⁻² y ⁻¹)	RMSE _{NEP} (gC m ⁻² d ⁻¹)	No. of years
1	650	616	0.67	40	45	0.70	2
2	1492	1421	1.13	397	427	1.02	4
3	619	614	0.64	53	54	0.56	4
4	2064	1875	1.42	279	251	1.25	4
5	1345	1314	1.21	16	37	1.40	4
6	3178	3127	1.61	-36	-40	1.35	2
7	677	771	1.15	74	69	0.85	1
8	1537	1478	2.60	501	517	2.19	2
9	1469	1472	1.48	383	385	1.45	2
10	1177	1196	1.31	168	163	1.23	2
11	329	407	0.66	180	186	0.57	2
12	NA	86	0.32	NA	-16	0.29	1
13	421	377	0.56	41	49	0.74	1
14	NA	168	0.44	NA	115	0.37	2
15	938	928	1.30	-42	-10	1.24	4
16	517	534	0.76	133	143	0.57	1
17	1191	1085	3.35	478	435	3.07	2
18	1205	1228	3.29	228	215	2.40	2

in CFLUX. Total respiration (R_e) shows a rather similar relation to WHC (Fig. 5), due to the assumption that autotrophic respiration is a constant fraction of GPP and the assumption that heterotrophic respiration declines as available soil moisture declines—albeit in a somewhat different fashion than does GPP. Across the 6 temperate PFDs of Table 4, GPP is insensitive to WHC, due to offsetting effects of soil moisture on GPP and R_e .

To illustrate the effects of shifts in temperature we added constant temperature increments to the minimum daily temperature, the average daily temperature and the soil temperature, as location-related shifts in climate are likely to affect all three temperature inputs. For evergreen forests subject to cold winters, such as the Rocky Mountains site, GPP increased substantially with increasing temperature, as there was less limitation of production by low night temperatures (Fig. 6). R_e also increased, as both of its two components (autotrophic and heterotrophic respiration) increase with temperature. Autotrophic respiration is assumed to be proportional to GPP (which increases with T_{min} on cold evergreen sites), whereas heterotrophic respiration increases with soil temperature. Annual NEP showed a considerably smaller shift with temperature, as the increases in GPP and R_e offset each other (Fig. 6).

For deciduous forests subject to cold winters, the effect of moderating cold night temperatures was mostly confined to the leafless season when the satellite FPAR driving GPP was low. Hence GPP was less sensitive to temperature than for evergreen forests and the resultant effect on NEP was also small (Table 4). In the case of the California annual grassland, annual GPP is largely limited by the depletion of soil water stores in mid spring, so temperature has a

small effect. A strong temperature effect on NEP was observed for the temperate maritime site of Table 4, due to high GPP and respiratory fluxes at this productive site and a strong temperature response of heterotrophic respiration here.

To illustrate the effects of shifts in VPD we multiplied the average VPD for each day by a constant factor ranging from 0.5 to 1.5. This approach prevents the negative VPDs that would occur with the subtraction of only a small increment of VPD on cool wet winter days. Also, the maximum VPDs are likely to show the greatest shifts in moving from wet to dry sites. Effects were small for the illustrated DBF site (Fig. 7), where VPDs are relatively low on most days and the VPD effect ramps up gradually from a VPD of 500 to 4000. An interaction with soil water limitation appeared to mute the effects of changing VPD for the California grassland, as reducing early spring GPP via higher VPDs delays the onset of soil water effects that depress GPP later in the season. Increasing VPD generally decreased modeled GPP more than it decreased R_e , resulting in moderate declines in predicted NEP (Table 4).

3.3. Comparison of cross site vs. single site optimizations

For the five PFT/climate zone combinations with multiple tower sites, the RMSE was generally lower at each site for site-specific parameter optimizations than when the site was run with parameters derived from a cross-site optimization (data not shown). However, across all sites within a PFT/climate zone combination, the RMSE was generally higher when a single site optimization was used at all sites than when this was done with the cross site optimization (Table 5).

Annual flux values derived from single site fits were likewise usually closer to reported values for the home sites than were those derived from multisite optimizations. When sites of differing productivities were involved there was a tendency for the cross site fit to under- and over-predict GPP at the more and less productive sites, respectively. However, the overall average values across years and sites derived from the cross site fits were substantially closer to the corresponding flux tower averages. (Mean predicted GPP per PFT ranged from -11 to +11% of the corresponding observed mean across the 5 PFTs with cross site fits.) That is, there was less systematic bias in the overall averaged estimates.

3.4. Comparison of fits to MODIS FPAR vs. EVI

The MODIS FPAR is consistently higher than the MODIS EVI for the evergreen sites (coniferous forests and chaparral). A comparison of

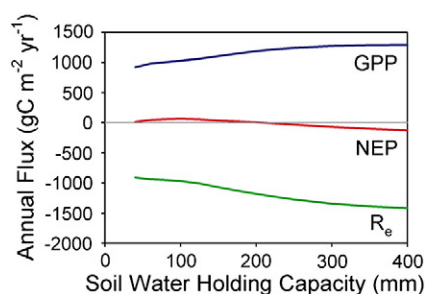


Fig. 5. Sensitivity of simulated fluxes to variation in soil WHC at site 15 (Temperate GRASS). R_e curve shown as negative in value for clarity. Estimated actual WHC = 100 mm at this site.

Table 4

Sensitivity of the model to temperature, soil water holding capacity and VPD for the 6 temperate PFTs and site-year runs of Fig. 2 (2005 corn year for CROP). Sensitivities are the changes in annual GPP, R_e and NEP due to a 10% increase in soil water holding capacity (WHC), a 1° increase in daily minimum temperature, daily average temperature and daily soil temperature (labeled T), and a 10% increase in daily VPD. Annual GPP, R_e and NEP are shown for comparison to the incremental changes. All values are in $\text{gC m}^{-2} \text{y}^{-1}$.

PFT	Annual	Sensitivity of GPP to			Annual	Sensitivity of R_e to			Annual	Sensitivity of NEP to		
	GPP	WHC	T	VPD	R_e	WHC	T	VPD	NEP	WHC	T	VPD
ENF	606	0	0	-30.6	562	0.5	20.8	-14.5	44	-0.5	10.7	-16.1
Maritime	1840	33.1	50.6	-4.9	1575	34.4	184.8	0.2	265	-1.3	-134.2	-5.1
DBF	1553	0.3	29.0	-26.8	1131	1.9	17.9	-12.6	422	-1.6	11.1	-14.2
SHRUB	441	0.3	5.9	-18.6	239	0.4	3.4	-9.1	202	-0.1	2.4	-9.5
GRASS	1026	11.0	6.8	-17.1	966	9.1	10.0	2.1	60	2.0	-3.2	-19.2
CROP	1409	29.7	32.0	-16.8	909	15.6	14.5	-2.8	-501	-5.6	17.5	-13.9

mean growing season MODIS FPAR and EVI with FPAR inferred from measurements of canopy leaf area for the BigFoot project (Turner et al., 2005) shows that the overall average EVI value was 37% lower than the measurement based estimates (Table 6). The MODIS FPAR was on average close to the Bigfoot values, though these two differed substantially at several sites.

Examples of MODIS FPAR and EVI (Fig. 8) show that the former averages 1–2 times higher than the latter. The two are quite similar for the illustrated crop site and show parallel increases during the growing season for the sites dominated by deciduous plants (crops, deciduous broadleaf forests and most grasslands). The seasonal dynamics in both FPAR sources are somewhat muted compared to the expected patterns for deciduous vegetation, although they do capture most of the seasonal variation. However a value close to zero is expected during the dormant season (dry season for California annual grasslands and winter for annual crops and deciduous forests).

The parameters determining the base light use efficiency (LUE_{cs} and LUE_{max}) were substantially higher when CFLUX was fit with EVI than with FPAR (Fig. 9). This pattern is expected, as the lower modeled light interception associated with EVI requires higher LUEs to achieve a given GPP. The base rate of heterotrophic respiration (R_{h_base}) was also higher for the EVI optimization (Fig. 9) because heterotrophic respiration is scaled to leaf area index, which is inferred from the FPAR or EVI input. The parameters defining the effect of low temperatures and VPD on LUE were generally similar for the EVI and FPAR optimizations.

The RMSE's associated with the EVI vs. MODIS FPAR optimizations were quite similar, despite the substantial differences in the resultant LUE parameters, both for single and multiple site optimizations (Table 7). The predicted annual values of GPP, R_e and NEP for EVI vs. MODIS FPAR were quite similar to each other—and to the observed flux tower values (Fig. 10). The deviations from the observed values for annual GPP and R_e were correlated with each other, resulting in smaller deviations in annual NEP. Thus, the two FPAR sources performed equally well. However, as the EVI values are often much lower than the actual FPAR values, the EVI-associated light use

efficiency parameters are biased upwards in comparison to true light use efficiencies calculated as $GPP/(\text{actual absorbed PAR})$.

4. Discussion

4.1. Site-level parameterization

The model parameter sets derived for the 18 sites varied substantially, most notably LUE_{cs} and LUE_{max} , which specify the base LUE under unstressed conditions. These parameters were correlated with annual GPP, particularly for the evergreen needleleaf forest sites (Tables 1–3). Mäkelä et al. (2008) also reported variation in base LUE for coniferous forest flux tower sites, and found that it correlated with foliar nitrogen concentration. The latter relation is in agreement with observed relations between photosynthetic capacity and leaf nitrogen concentration (Evans, 1989; Reich et al., 1997). The LUE parameters were quite low for the low-productivity SHRUB and Arctic GRASS sites.

The base rate of heterotrophic respiration (R_{h_base}) also varied greatly among sites and tended to increase with annual GPP (Tables 2 and 3). However, the high temperature dependence of R_h for the three evergreen conifer sites of the Pacific Northwest resulted in the model fitting high summertime respiration rates with modest values of R_{h_base} .

The RMSE errors in daily GPP and NEP showed moderate sensitivity to variation in the optimized parameters about their optimal values (Fig. 3). In cases where the optima lay at the boundary of the searched parameter space, the RMSE decreased to varying extents in crossing the boundary at the point of the optimum. However, the predicted annual values of GPP, R_e and NEP were quite close to the observed values for most sites (Fig. 10).

CFLUX is a relatively simple diagnostic model, designed for rapid simulations when run in the spatial mode. Consequently, the model mechanisms fitting the tower data aren't the full component of environmental factors that may affect carbon fluxes across all sites. For example, the model includes the effects of cold nights on LUE, but

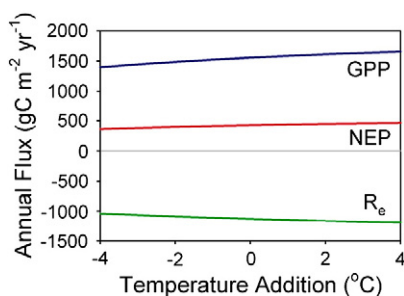


Fig. 6. Sensitivity of simulated fluxes to variation in temperature at site 9 (Temperate DBF). T_{min} , T_{avg} and T_{soil} were all varied by the amount on shown on the x-axis for each day of a representative year. R_e curve shown as negative in value for clarity.

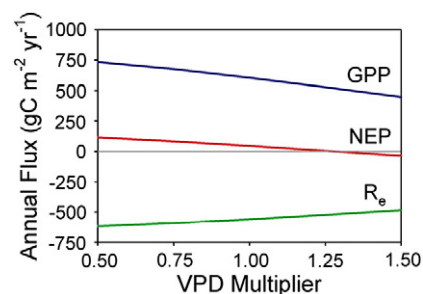


Fig. 7. Sensitivity of simulated fluxes to variation in VPD at site 3 (Temperate ENF). Observed VPD was multiplied by the indicated factor for each day of a representative year. R_e curve shown as negative in value for clarity.

Table 5

Simulated annual fluxes, associated biases, and daily RMSEs for the temperate deciduous broadleaf PFT, as derived from parameterizations for each site and across all sites. GPP bias is mean annual simulated GPP over all sites and years (Column 2) minus the mean annual observed GPP across all sites and years. $RMSE_{GPP}$ refers to the RMSE for daily GPP across all sites and years. The same information is given for NEP. Sites are defined in Table 1.

Parameterization site	All site mean annual GPP ($gC\ m^{-2}\ y^{-1}$)	GPP bias ($gC^{-2}\ y^{-1}$)	All site $RMSE_{GPP}$ ($gC\ m^{-2}\ d^{-1}$)	All site mean annual NEP ($gC\ m^{-2}\ y^{-1}$)	NEP bias ($gC\ m^{-2}\ y^{-1}$)	All site $RMSE_{NEP}$ ($gC\ m^{-2}\ d^{-1}$)
8	1483	89	2.46	530	179	1.95
9	1234	-160	2.16	271	-80	1.92
10	1275	-119	2.13	174	-177	1.95
Cross site	1386	-8	2.04	363	12	1.81

Table 6

Comparison of mid growing season FPAR (as estimated from BigFoot LAI observations, Turner et al., 2005) with MODIS FPAR and MODIS EVI. Values are means across years (where relevant) and over multiple 1 km grid cells at each site. Sites are defined in Table 1.

Site number/years	BigFoot	MODIS FPAR	MODIS EVI
8/2001–2003	0.86	0.81	0.55
2/2002	0.47	0.67	0.30
1/2001	0.89	0.66	0.29
6/2002	0.95	0.76	0.53
14/2002–2003	0.11	0.15	0.12
12/2002	0.30	0.35	0.25
17/2000	0.67	0.70	0.63
Average	0.61	0.59	0.42

no effects of daytime temperatures. Some other production models employ a quadratic function that reduces LUE when daytime temperatures are either above or below an optimal value (Sands, 1995; Yuan et al., 2007). However, VPD also tends to be high on hot days and daily minimum temperatures are low on cold days. Thus, the fitted VPD and T_{min} effects may also serve as surrogates for additional daytime temperature effects on LUE.

Probably the greatest simplification within CFLUX is with respect to R_h . In forests, rates of R_h are undoubtedly different in litter, coarse woody debris, and soil organic matter on any given day. The contribution of coarse woody debris to R_h will also vary with stand development (Bond-Lamberty & Gower, 2008). For the old-growth evergreen needleleaf forest in the Cascade Mountains of Washington (site 5), respiration from large downed logs is also a significant CO_2 source (Harmon et al., 2004), which shows a different dependence on moisture content than do soils and small woody debris (Carpenter et al., 1988). Unlike the latter, logs show arrested respiration when

saturated with water and increased respiration in late summer, as they dry out in the Pacific Northwest. This additional source of warm season respiration may be captured by the high temperature dependence of R_h at this site, as fit by CFLUX.

4.2. Cross-site parameterization

Within each PFT, the parameter sets derived from cross-site optimizations performed substantially better at predicting the annual NEP, as averaged across all sites and years than did the individual site parameter sets (Table 5). However, the individual site optimizations generally had lower RMSE's for their respective home sites than did the cross site optimization, as expected. Possible reasons for biases in the predictions of site optimized parameter sets when applied to different sites within a PFT include:

1. Intersite differences not included in CFLUX, such as soil fertility and species composition, which may affect LUE (Kirschbaum et al., 1994). The difference between the LUE of corn and soybean (Fig. 2), due to differences in photosynthetic pathway (C_4 vs. C_3), and the carbon and energy content of the biomass of these two crops is perhaps an extreme example, but variation in LUE among other crop species has also been reported (Choudbury, 2001). Likewise, the photosynthetic capacity of trees varies substantially among genotypes and species, although the relation between leaf photosynthetic capacity and whole-stand productivity is complex (Pallardy & Kozlowski, 2008).
2. Error in the estimates of fluxes derived from eddy flux correlations, associated with differences in topography and tower footprints among sites (Aubinet, 2008; Baldocchi, 2003).
3. Error in satellite-based FPAR due to cloud contamination and other factors (Nagai et al., 2010), which may vary among sites.

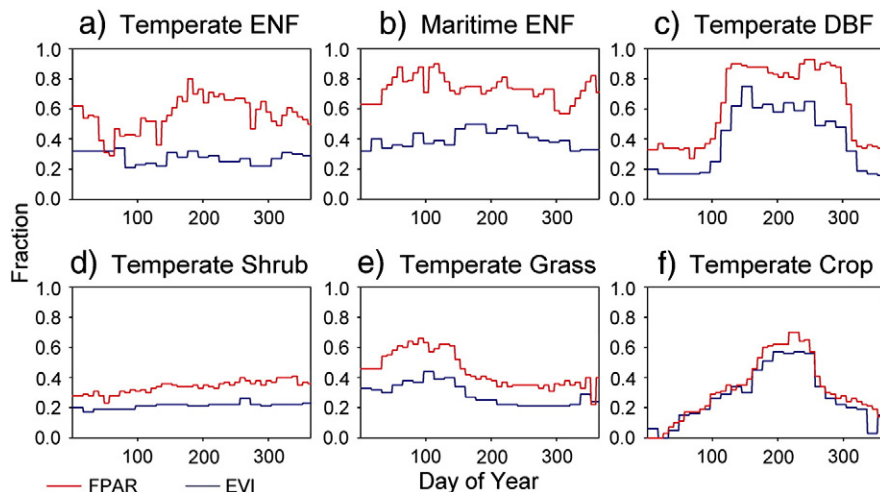


Fig. 8. Comparison of FPAR and EVI time series, indicated by red and blue lines, respectively (for all panels the EVI trace is below the FPAR trace in midseason). Site and years are the same as in Fig. 4.

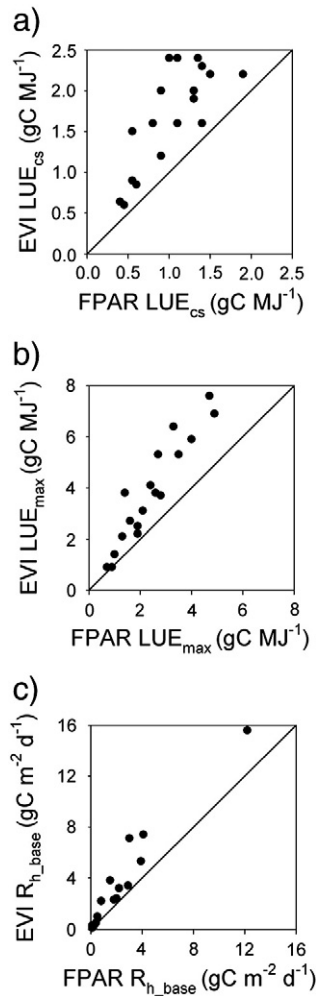


Fig. 9. Comparison of EVI and FPAR parameters. LUE_{cs} is light use efficiency under unstressed clear sky conditions, LUE_{max} is maximum light use efficiency, R_{h_base} is the base rate of heterotrophic respiration.

4.3. Comparison of FPAR and EVI

Despite substantive differences between the MODIS FPAR and EVI inputs, CFLUX showed similar errors in fitting the parameters to these two inputs and quite similar projections of annual fluxes (Fig. 10). The optimization of the parameters may also correct for deficiencies in the input data for both FPAR and EVI inputs. For example, the optimized $FPAR_{min}$, the minimum FPAR driving heterotrophic respiration, was always ≥ 0.5 and often = 1, which would negate spuriously low values in the satellite FPAR estimates, due to clouds, snow cover and other causes. This capacity to implicitly handle additional processes and environmental effects and adjust to differences in input data is a strength of diagnostic models.

Table 7

Comparison of RMSEs for cross site optimizations with MODIS FPAR and MODIS EVI. ENF = Evergreen Needleleaf Forest, DBF = Deciduous Broadleaf Forest.

PFT	RMSE _{C_{PP}} (gC m ⁻² d ⁻¹)		RMSE _{NEP} (gC m ⁻² d ⁻¹)		No. sites	Years per site
	FPAR	EVI	FPAR	EVI		
Maritime ENF	1.55	1.50	1.69	1.64	2	4
Temperate ENF	1.44	1.27	1.09	1.04	2	4
Temperate DBF	2.04	2.01	1.81	1.79	3	2
Temperate GRASS	0.91	0.99	0.98	1.00	3	1
Temperate CROP	3.44	3.45	2.79	2.91	2	2

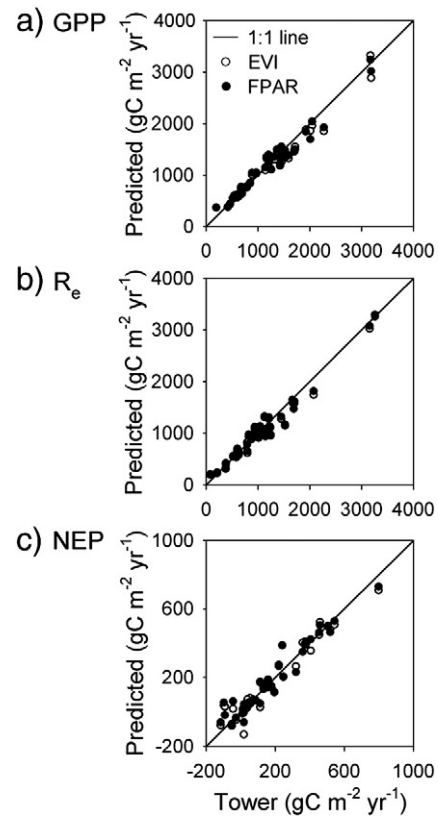


Fig. 10. Comparison of predicted annual fluxes with EVI and FPAR inputs after optimization of the model parameters to these respective inputs for each site.

4.4. Towards continental scale model application

The performance of CFLUX when fit to disparate FPAR inputs and its response to varying meteorological inputs and soil water holding capacity show it to be a robust and flexible model which produces relatively stable estimates of annual NEP. Using a level of disaggregation characterized by 3 climate zones and 6 plant functional types, we were able to find one or more representative tower sites in almost all the climate zone \times PFT classes. We have applied the model in the spatial mode over western Oregon (Turner et al., 2006) and produced NEP flux estimates that compared well to those produced by a more process-based model (Biome-BGC). Notably, the diagnostic model is able to account to some degree for the effects of recent large scale forest fires, sub-regional patterns in stand age, and interannual variation in climate on NEP. Application at the continental scale will rely on distributed climate data and recently available input datasets such as the stand age coverage of Pan et al. (2011). Opportunities for validation at broad spatial scales include additional model intercomparison studies (e.g. Cramer et al., 1999) and input of simulated NEP to inversion schemes that evaluate predicted and measured CO₂ concentration data (Ahmadov et al., 2009). Our analysis suggests that the cross site parameter fits for PFD/climate zones with multiple sites should produce less bias in overall annual carbon fluxes than fits to individual sites.

Acknowledgments

This research was supported by the NASA Terrestrial Ecology Program (NNX09AL51G). Data from the AmeriFlux and FluxNet networks and the Oak Ridge National Laboratory Distributed Active Archive Center for Biogeochemical Dynamics were essential for the completion of this study. We thank the flux tower investigators and support personnel for tower data acquisition and assembly.

References

- Ahmadov, R., Gerbig, C., Kretschmer, R., Korner, S., Rodenbeck, C., Bousquet, P., et al. (2009). Comparing high resolution WRF-VRM simulations and two global CO₂ transport models with coastal tower measurements of CO₂. *Biogeosciences*, 6, 807–817.
- Alton, P. B., North, P. R., & Los, O. (2007). The impact of diffuse sunlight on canopy light-use efficiency, gross photosynthetic product and net ecosystem exchange in three forest biomes. *Global Change Biology*, 13, 776–787.
- AmeriFlux (2011). <http://public.ornl.gov/ameriflux/>.
- Atkin, O. K., & Tjoelker, M. G. (2003). Thermal acclimation and the dynamic response of plant respiration to temperature. *Trends in Plant Science*, 8, 343–351.
- Aubinet, M. (2008). Eddy covariance CO₂ flux measurements in nocturnal conditions: An analysis of the problem. *Ecological Applications*, 18, 1368–1378.
- Baldocchi, D. D. (2003). Assessing the eddy covariance technique for evaluating carbon dioxide exchange rates of ecosystems: Past, present and future. *Global Change Biology*, 9, 479–492.
- Baldocchi, D., Falge, E., Gu, L., Olson, R., Hollinger, D., Running, S., et al. (2001). FLUXNET: A new tool to study the temporal and spatial variability of ecosystem-scale carbon dioxide, water vapor, and energy flux densities. *Bulletin of the American Meteorological Society*, 82, 2415–2434.
- Bond-Lamberty, B., & Gower, S. T. (2008). Decomposition and fragmentation of coarse woody debris: Revisiting a boreal black spruce chronosequence. *Ecosystems*, 11, 831–840.
- Carpenter, S. E., Harmon, M. E., Ingham, E. R., Kelsey, R. G., Lattin, J. D., & Schowalter, T. D. (1988). Early patterns of heterotrophy activity in conifer logs. *Proceedings. Royal Society of Edinburgh*, 94B, 33–43.
- Choudbury, B. J. (2001). Estimating gross photosynthesis using satellite and ancillary data: Approach and preliminary results. *Remote Sensing of Environment*, 75, 1–21.
- Cramer, W., Kicklighter, D. W., Bondeau, A., Moore, B., III, Churkina, G., Nemry, B., et al. (1999). Comparing global models of terrestrial net primary production (NPP): Overview and key results. *Global Change Biology*, 5(Suppl. 1), 1–15.
- da Rocha, H. R., Goulden, M. L., Miller, S. D., Menton, M. C., Pinto, L. D. V. O., de Freitas, H. C., et al. (2004). Seasonality of water and heat fluxes over a tropical forest in Eastern Amazonia. *Ecological Applications*, 14(4), S22–S32 Supplement.
- De Lucia, E. H., Drake, J. E., Thomas, R. B., & Gonzalez-Melers, M. (2007). Forest carbon use efficiency: Is respiration a constant fraction of gross primary production? *Global Change Biology*, 13, 1157–1167.
- Dunn, A. L., Barford, C. C., Wofsy, S. C., Goulden, M. L., & Daube, B. C. (2007). A long-term record of carbon exchange in a boreal black spruce forest: Means, responses to interannual variability, and decadal trends. *Global Change Biology*, 13, 577–590.
- Evans, J. R. (1989). Photosynthesis and nitrogen relationships in leaves of C₃ plants. *Oecologia*, 78, 9–19.
- Falk, M., Wharton, S., Schroeder, M., Ustin, S. L., & Paw, U. K. T. (2008). Flux partitioning in an old-growth forest: Seasonal and interannual dynamics. *Tree Physiology*, 28, 509–520.
- Friedl, M. A., Sulla-Menashe, D., Tan, B., Schneider, A., Ramankutty, N., Sibley, A., et al. (2010). MODIS Collection 5 global land cover: Algorithm refinements and characterization of new datasets. *Remote Sensing of Environment*, 114, 168–182.
- Fu, P., & Rich, P. M. (1999). Design and implementation of the Solar Analyst: An ArcView extension for modeling solar radiation at landscape scales. *Proceedings of the 19th Annual ESRI User Conference*. San Diego, USA. <http://gis.esri.com/library/userconf/proc99/proceed/papers/pap867/p867.htm> Accessed 3/1/2011.
- Garbulska, M. E., Peñuelas, J., Papale, D., Ardö, J., Goulden, N. L., Kiely, G., et al. (2010). Patterns and controls of the variability of radiation use efficiency and primary productivity across terrestrial ecosystems. *Global Ecology and Biogeography*, 19, 253–267.
- Gilmanov, T. G., Tieszen, L. L., Wylie, B. K., Flanagan, L. B., Frank, A. B., Haferkamp, M. R., et al. (2005). Integration of CO₂ flux and remotely-sensed data for primary production and ecosystem respiration analyses in the Northern Great Plains: Potential for quantitative spatial extrapolation. *Global Ecology and Biogeography*, 14, 271–292.
- Göckede, M., Michalak, A. M., Vickers, D., Turner, D. P., & Law, B. E. (2010a). Atmospheric inverse modeling to constrain regional-scale CO₂ budgets at high spatial and temporal resolution. *Journal of Geophysical Research, [Atmospheres]*, 115, D15113.
- Göckede, M., Turner, D. P., Michalak, A. M., Vickers, D., & Law, B. E. (2010b). Sensitivity of a subregional scale atmospheric inverse CO₂ modeling framework to boundary conditions. *Journal of Geophysical Research, [Atmospheres]*, 115, D24112.
- Gower, S. T., Kucharik, C. J., & Norman, J. M. (1999). Direct and indirect estimation of leaf area index, fAPAR and net primary production of terrestrial ecosystems. *Remote Sensing of Environment*, 70, 29–51.
- Harmon, M. E., Bible, K., Ryan, M. G., Shaw, D. C., Chen, H., Klopatek, J., et al. (2004). Production, respiration, and overall carbon balance in an old-growth *Pseudotsuga-Tsuga* forest ecosystem. *Ecosystems*, 7, 498–512.
- Haxeltine, A., & Prentice, I. C. (1996). A general model for light-use efficiency of primary production. *Functional Ecology*, 10, 551–561.
- Hogberg, P., Nordgren, A., Buchmann, N., Taylor, F. S., Ekblad, A., Hogberg, N. M., et al. (2001). Large-scale forest girdling shows that current photosynthate drives soil respiration. *Nature*, 411, 789–792.
- Hollinger, D. Y., Kelliher, F. M., Byers, J. N., Hunt, J. E., McSevery, T. M., & Weir, P. L. (1994). Carbon dioxide exchange between an undisturbed old-growth temperate forest and the atmosphere. *Ecology*, 75, 134–150.
- Huete, A., Didan, K., Miura, T., Rodriguez, E. P., Gao, X., & Ferreira, L. G. (2002). Overview of the radiometric and biophysical performance of the MODIS vegetation indices. *Remote Sensing of Environment*, 83, 195–213.
- Kennedy, R. E., Cohen, W. B., & Schroeder, T. A. (2007). Trajectory-based change detection for automated characterization of forest disturbance dynamics. *Remote Sensing of Environment*, 110, 370–386.
- Kirschbaum, M. U. F., King, D. A., Comins, H. N., McMurtrie, R. E., Medlyn, B. E., Keith, H., et al. (1994). Modelling forest response to increasing CO₂ concentration under nutrient-limited conditions. *Plant, Cell & Environment*, 17, 1081–1099.
- Krishnan, P., Black, T. A., Jassal, R. S., Chen, B. Z., & Nescic, Z. (2009). Interannual variability of the carbon balance of three different-aged Douglas-fir stands in the Pacific Northwest. *Journal of Geophysical Research, Biogeosciences*, 114(G04011), doi:10.1029/2008JG000912.
- Kurc, S. A., & Small, E. E. (2007). Soil moisture variations and ecosystem-scale fluxes of water and carbon in semiarid grassland and shrubland. *Water Resources Research*, 43(W06416), doi:10.1029/2006WR005011.
- Kwon, H. J., Oechel, W. C., Zulueta, R. C., & Hastings, S. J. (2006). Effects of climate variability on carbon sequestration among adjacent wet sedge tundra and moist tussock tundra ecosystems. *Journal of Geophysical Research, Biogeosciences*, 111(G03014), doi:10.1029/2005jg000036.
- Law, B. E., Falge, E., Gu, L., Baldocchi, D. D., Bawkin, P., Berbigier, P., et al. (2002). Environmental controls over carbon dioxide and water vapor exchange of terrestrial vegetation. *Agricultural and Forest Meteorology*, 113, 97–120.
- Licata, J. A., Gyenge, J. E., Fernandez, M. E., Schlichter, T. M., & Bond, B. J. (2008). Increased water use by ponderosa pine plantations in northwestern Patagonia, Argentina compared with native forest vegetation. *Forest Ecology and Management*, 255, 753–764.
- Luo, H. Y., Oechel, W. C., Hastings, S. J., Zulueta, R., Qian, Y. H., & Kwon, H. (2007). Mature semiarid chaparral ecosystems can be a significant sink for atmospheric carbon dioxide. *Global Change Biology*, 13, 386–396.
- Ma, S., Baldocchi, D. D., Xu, L., & Hehn, T. (2007). Inter-annual variability in carbon dioxide exchange of an oak/grass savanna and open grassland in California. *Agricultural and Forest Meteorology*, 147, 157–171.
- Mahadevan, P., Wofsy, S. C., Matross, D. M., Xiao, X. M., Dunn, A. L., Lin, J. C., et al. (2008). A satellite-based biosphere parameterization for net ecosystem CO₂ exchange: Vegetation Photosynthesis and Respiration Model (VPRM). *Global Biogeochemical Cycles*, 22(GB2005), doi:10.1029/2006GB002735.
- Mäkelä, A., Pulkkinen, M., Kolari, P., Lagergren, F., Berbigier, P., Lindroth, A., et al. (2008). Developing an empirical model of stand GPP with the LUE approach: Analysis of eddy covariance data at five contrasting conifer sites in Europe. *Global Change Biology*, 14, 92–108.
- Matross, D. M., Andrews, A., Pathmathevan, M., Gerbig, C., Lin, J. C., Wofsy, S. C., et al. (2006). Estimating regional carbon exchange in New England and Quebec by combining atmospheric, ground-based and satellite data. *Tellus Series B-Chemical and Physical Meteorology*, 58, 344–358.
- McCallum, I., Wagner, W., Schullius, C., Shvidenko, A., Obersteiner, M., Fritz, S., et al. (2009). Satellite-based terrestrial production efficiency modeling. *Carbon Balance and Management*, 4(8), doi:10.1186/1750-0680-4-8.
- Meyers, T. P., & Hollinger, S. E. (2004). An assessment of storage terms in the surface energy balance of maize and soybean. *Agricultural and Forest Meteorology*, 125, 105–115.
- Monson, R. K., Turnipseed, A. A., Sparks, J. P., Harley, P. C., Scott-Denton, L. E., Sparks, K., et al. (2002). Carbon sequestration in a high-elevation, subalpine forest. *Global Change Biology*, 8, 459–478.
- Myneni, R., Hoffman, R., Knyazikhin, Y., Privette, J., Glassy, J., & Tian, H. (2002). Global products of vegetation leaf area and fraction absorbed PAR from one year of MODIS data. *Remote Sensing of Environment*, 76, 139–155.
- Nagai, S., Saigusa, N., Muraoka, H., & Nasahara, K. N. (2010). What makes the satellite-based EVI-GPP relationship unclear in a deciduous broad-leaved forest? *Ecological Research*, 25, 359–365.
- Nepstad, D. C., de Carvalho, C. R., Davidson, E. A., Jipp, P. H., Lefebvre, P. A., Negreiros, G. H., et al. (1994). The role of deep roots in the hydrological and carbon cycles of Amazonian forests and pastures. *Nature*, 372, 666–669.
- Oliver, W. W., & Ryker, R. A. (1990). *Pinus ponderosa* Dougl. ex Mill.—Ponderosa Pine. In R. M. Burns, & B. H. Honkala (Eds.), *Silvics of North America, Vol. 1, Conifers* (pp. 413–424). Washington: USDA Forest Service Agriculture Handbook 654.
- Omernik, J. M. (1987). Ecoregions of the conterminous United States. Map (scale 1: 7,500,000). *Annals of the Association of American Geographers*, 77, 118–125.
- ORNL (Oak Ridge National Laboratory Distributed Active Archive Center) (2010). *MODIS subsetted land products, Collection 5*. Available on-line. <http://daac.ornl.gov/MODIS/modis.html> from ORNL DAAC, Oak Ridge, Tennessee, U.S.A. Accessed 2/1/2010.
- Pallardy, S. G., & Kozlowski, T. T. (2008). *Physiology of woody plants* (3rd ed.). Burlington, MA: Academic Press, Elsevier, Inc.
- Pan, Y., Chen, J. M., Birdsey, R., McCullough, K., He, L., & Deng, F. (2011). Age structure and disturbance legacy of North American forests. *Biogeosciences*, 8, 715–732.
- Potter, C. S., Randerson, J. T., Field, C. B., Matson, P. A., Vitousek, P. M., Mooney, H. A., et al. (1993). Terrestrial ecosystem production, a process model based on global satellite and surface data. *Global Biogeochemical Cycles*, 7, 811–841.
- Reich, P. B., Walters, M. B., & Ellsworth, D. S. (1997). From tropics to tundra: Global convergence in plant functioning. *Proceedings of the National Academy of Science USA*, 94, 13730–13734.
- Running, S. W., Baldocchi, D. D., Turner, D. P., Gower, S. T., Bakwin, P. S., & Hibbard, K. A. (1999). A global terrestrial monitoring network integrating tower fluxes, flask sampling, ecosystem modeling and EOS satellite data. *Remote Sensing of Environment*, 70, 108–128.
- Running, S. W., Thornton, P. E., Nemani, R., & Glassy, J. M. (2000). Global terrestrial gross and net primary productivity from the Earth Observing System. In O. E. Sala, R. B. Jackson, H. A. Mooney, & R. W. Howarth (Eds.), *Methods in ecosystem science* (pp. 44–57). New York: Springer-Verlag.
- Saleska, S. R., Miller, S. D., Matross, D. M., Goulden, M. L., Wofsy, S. C., da Rocha, H. R., et al. (2003). Carbon in Amazon forests: Unexpected seasonal fluxes and disturbance-induced losses. *Science*, 302(5650), 1554–1557.

- Sands, P. J. (1995). Modelling canopy production. II. From single-leaf photosynthetic parameters to daily canopy photosynthesis. *Australian Journal of Plant Physiology*, 22, 603–614.
- Schmid, H. P., Grimmer, C. S. B., Cropley, F., Offerle, B., & Su, H. B. (2000). Measurements of CO₂ and energy fluxes over a mixed hardwood forest in the mid-western United States. *Agricultural and Forest Meteorology*, 103, 357–374.
- Schmid, H. P., Su, H. B., Vogel, C. S., & Curtis, P. S. (2003). Ecosystem-atmosphere exchange of carbon dioxide over a mixed hardwood forest in northern lower Michigan. *Journal of Geophysical Research, Atmospheres*, 108(4417), doi:10.1029/2002JD003011.
- Thomas, C. K., Law, B. E., Irvine, J., Martin, J. G., Pettijohn, J. C., & Davis, K. J. (2009). Seasonal hydrology explains interannual and seasonal variation in carbon and water exchange in a semiarid mature ponderosa pine forest in central Oregon. *Journal of Geophysical Research, Biogeosciences*, 114(G04006), doi:10.1029/2009JG001010.
- Thornton, P. E., Law, B. E., Gholz, H. L., Clark, K. L., Falge, E., Ellsworth, D. S., et al. (2002). Modeling and measuring the effects of disturbance history and climate on carbon and water budgets in evergreen needleleaf forests. *Agricultural and Forest Meteorology*, 113, 185–222.
- Turner, D. P., Ollinger, S. V., & Kimball, J. S. (2004). Integrating remote sensing and ecosystem process models for landscape to regional scale analysis of the carbon cycle. *Bioscience*, 54, 573–584.
- Turner, D. P., Ritts, W. D., Cohen, W. B., Maeirsperger, T. K., Gower, S. T., Kirschbaum, A., et al. (2005). Site-level evaluation of satellite-based global terrestrial gross primary production and net primary production monitoring. *Global Change Biology*, 11, 666–684.
- Turner, D. P., Ritts, W. D., Styles, J. M., Yang, Z., Cohen, W. B., Law, B. E., et al. (2006). A diagnostic carbon flux model to monitor the effects of disturbance and interannual variation in climate on regional NEP. *Tellus*, 58B, 476–490.
- Turner, D. P., Ritts, W. D., Wharton, S., Thomas, C., Monson, R., Black, T. A., et al. (2009). Assessing FPAR source and parameter optimization scheme in application of a diagnostic carbon flux model. *Remote Sensing of Environment*, 113, 1529–1539.
- Turner, D. P., Urbanski, S., Wofsy, S. C., Bremer, D. J., Gower, S. T., & Gregory, M. (2003). A cross-biome comparison of light use efficiency for gross primary production. *Global Change Biology*, 9, 383–395.
- Urbanski, S., Barford, C., Wofsy, S., Kucharik, C., Pyle, E., Budney, J., et al. (2007). Factors controlling CO₂ exchange on timescales from hourly to decadal at Harvard Forest. *Journal of Geophysical Research, Biogeosciences*, 112(G02020), doi:10.1029/2006JG000293.
- Verma, S. B., Dobermann, A., Cassman, K. G., Walters, D. T., Knops, J. M., Arkebauer, T. J., et al. (2005). Annual carbon dioxide exchange in irrigated and rainfed maize-based agroecosystems. *Agricultural and Forest Meteorology*, 131, 77–96.
- Wang, Y. P., Trudinger, C. M., & Enting, I. G. (2009). A review of applications of model-data fusion to studies of terrestrial carbon fluxes at different scales. *Agricultural and Forest Meteorology*, 149, 1829–1842.
- Wu, C., Munger, J. W., Niu, Z., & Kuang, D. (2010). Comparison of multiple models for estimating gross primary production using MODIS and eddy covariance data in Harvard Forest. *Remote Sensing of Environment*, 114, 2925–2939.
- Xiao, J. F., Zhuang, Q. L., Law, B. E., Baldocchi, D. D., Chen, J. Q., Richardson, A. D., et al. (2010). Assessing net ecosystem carbon exchange of U S terrestrial ecosystems by integrating eddy covariance flux measurements and satellite observations. *Agricultural and Forest Meteorology*, 151, 60–69.
- Yuan, W., Liu, S., Zhou, G., Zhou, G., Tieszen, L., Baldocchi, D., et al. (2007). Deriving a light use efficiency model from eddy covariance flux data for predicting daily gross primary production across biomes. *Agricultural and Forest Meteorology*, 143, 189–207.
- Zhang, X. Y., Friedl, M. A., & Schaaf, C. B. (2006). Global vegetation phenology from Moderate Resolution Imaging Spectroradiometer (MODIS): Evaluation of global patterns and comparison with in situ measurements. *Journal of Geophysical Research, Biogeosciences*, 111(G04017), doi:10.1029/2006JG000217.
- Zhao, M. S., Heinsch, F. A., Nemani, R. R., & Running, S. W. (2005). Improvements of the MODIS terrestrial gross and net primary production global data set. *Remote Sensing of Environment*, 95, 164–176.